SCIENTIFIC REPORTS

OPEN

SUBJECT AREAS:
CATALYSIS
HETEROGENEOUS CATALYSIS

Received
6 August 2013

Accepted
7 November 2013

Published
22 November 2013

Correspondence and requests for materials should be addressed to Y.-J.X. (yjxu@fzu.edu.cn)

Visible-Light-Driven Oxidation of Primary C–H Bonds over CdS with Dual Co-catalysts Graphene and TiO_2

Min-Quan Yang[1,2], Yanhui Zhang[1,2], Nan Zhang[1,2], Zi-Rong Tang[2] & Yi-Jun Xu[1,2]

[1]State Key Laboratory Breeding Base of Photocatalysis, College of Chemistry and Chemical Engineering, Fuzhou University, Fuzhou, 350002, P. R. China, [2]College of Chemistry and Chemical Engineering, New Campus, Fuzhou University, Fuzhou, 350108, P. R. China.

Selective activation of primary C–H bonds for fine chemicals synthesis is of crucial importance for the sustainable exploitation of available feedstocks. Here, we report a viable strategy to synthesize ternary GR-CdS-TiO_2 composites with an intimate spatial integration and sheet-like structure, which is afforded by assembling two co-catalysts, graphene and TiO_2, into the semiconductor CdS matrix with specific morphology as a visible light harvester. The GR-CdS-TiO_2 composites are able to serve as a highly selective visible-light-driven photocatalyst for oxidation of saturated primary C–H bonds using benign oxygen as oxidant under ambient conditions. This work demonstrates a wide, promising scope of adopting co-catalyst strategy to design more efficient semiconductor-based photocatalyst toward selective activation of C–H bonds using solar light and molecular oxygen.

Selective oxidation of saturated sp^3 C–H bonds has been remaining a significant and challenging task in both fundamental and chemical industry toward the exploitation of available feedstocks in a sustainable manner[1–8]. However, selective oxidation of C–H bonds with environmentally benign oxygen is often very difficult to control because the activation of very inert C–H bonds typically requires harsh reaction conditions, *e.g.*, high pressure and high temperature; with such reaction conditions, the reactivity of molecular oxygen is difficult to control, thereby resulting in poor selectivity or overoxidation. Commercial processes for selective oxidation of such C–H bonds are often based on thermocatalytic approaches involving the use of metal catalysts, high temperature and/or high pressure[9]. Recent years have witnessed significant progress regarding heterogeneous thermocatalytic selective oxidation of C–H bonds, which includes selective oxidation of primary C–H bonds in toluene over alloyed Au-Pd nanoparticles supported on carbon or TiO_2 and metal-free g-C_3N_4 polymer with nanopores, and selective oxidation of secondary C–H bonds in cyclohexane over metal-free nanocomposites of graphene nanosheets and C_3N_4 polymer[9,10]. Notably, the use of harsh reaction conditions, high temperature (150 $\sim$ 160°C) and high pressure (10 bar oxygen pressure), are still required for these heterogeneous thermocatalytic selective oxidation of inert C–H bonds[9,10].

Heterogeneous photocatalysis by semiconductor-based materials features the unique advantages of operation under room temperature and utilization of clean, renewable solar light as the driving force[11–26]. Therefore, heterogeneous photocatalysis under ambient conditions and visible light represents an attractive, promising alternative for selective activation of C–H bonds[27–30]. Fukuzumi and co-workers have reported selective oxidation of primary C–H bonds in *p*-xylene to produce *p*-tolualdehyde in an O_2-saturated acetonitrile solvent over an Acr^+-Mes@AlMCM-41 composite; and the formation of a long-lived electron-transfer (ET) state in Acr^+-Mes@AlMCM-41 upon visible light irradiation affords the enhanced photocatalytic oxygenation reactivity[27]. Zhu's group has demonstrated aerobic selective oxidation of primary C–H bonds in toluene and its derivatives in benzotrifluoride (BTF) solvent to generate aldehydes, alcohols and acids over metal hydroxide nanoparticles grafted with alcohols under visible light irradiation, albeit the photoactivity is still low[28]. Free radicals formed on the surface complexes grafted onto metal hydroxides have been proposed to initiate the activation of C–H bonds in alkyl aromatics[28]. Similarly, Yuan and co-workers recently have shown a chlorine-radical-mediated visible-light-driven photocatalytic activation of C–H bonds in alkyl aromatics and cyclohexane in BTF solvent and even solvent-free conditions over surface-chlorinated BiOBr/TiO_2 composites (CBT)[29].

Very recently, our group has reported that tuning the microstructure and morphology composition in a very simple way is able to transform the well-known semiconductor CdS into an efficient visible light photocatalyst for

oxidation of primary C–H bonds with dioxygen as benign oxidant[30]. In particular, the as-prepared cubic phase, sheet structured CdS is extremely selective for aerobic oxidation of primary C–H bonds in toluene and substituted toluenes to corresponding aldehydes. However, similar to previous research works[27–29], the low photoactivity of CdS highlights the fact that there is still a need to improve the photocatalytic performance of CdS for selective oxidation of C–H bonds. Thus, the optimization of light capture, separation and transfer of photogenerated charge carriers over the semiconductor CdS surface is of vital importance toward the achievement of enhanced photoactivity of CdS for C–H activation under visible light. In this regard, the strategy of constructing spatial integration of semiconductor and co-catalysts to form composite materials in an appropriate manner is potentially useful to enhance the photoactivity of semiconductor CdS, because the co-catalysts are able to cooperate with the light harvester to facilitate the charge separation/transfer and lengthen the lifetime of photogenerated electron-hole pairs, thereby resulting in an increase in the overall photocatalytic performance[31–33].

Graphene (GR), a single layer of graphite, has superior electron conductivity/mobility and been shown to be an efficient co-catalyst to assemble with semiconductors to form graphene-semiconductor composite photocatalysts, which can exhibit enhanced photoactivity in solar energy conversion, *e.g.*, photocatalytic pollutants degradation, water splitting, CO_2 reduction and selective oxidation of alcohols[20,21,34]. On the other hand, the intrinsic energy band structure match between CdS and wide-band-gap TiO_2 indicates the feasibility of directional migration of photogenerated electrons from CdS to the conduction band (CB) of TiO_2 under visible light irradiation[35]. Thus, in principle, if CdS is hybridized with two co-catalysts of graphene and TiO_2 in a proper manner, the lifetime and transfer of photogenerated charge carriers, *i.e.*, electron-hole pairs, would be efficiently improved. Consequently, it can be expected that the photoactivity of CdS toward C–H activation would be enhanced effectively. Toward this purpose, we herein demonstrate a viable strategy of assembling two co-catalysts, graphene and TiO_2, with visible-light-active semiconductor CdS toward an improved photoactivity for aerobic selective C–H activation under mild conditions, room temperature and atmospheric pressure.

Results

We initially have prepared GR-CdS composites aiming to (i) determine the optimal ratio of GR in order to get an optimal enhancement of CdS photoactivity toward aerobic C–H oxidation *via* the addition of GR as a co-catalyst (for synthesis details, see Supplementary Information) and (ii) provide a basis for further constructing ternary GR-CdS-TiO_2 composites as discussed later. The CdS sample was synthesized by a very simple wet chemistry method at room temperature[30]. As shown in Figure S1 (Supplementary Information), all the GR-CdS composites with different weight addition ratios of GR, *i.e.*, 1, 5, 10 and 30% GR-CdS, show similar XRD patterns with that of blank-CdS sample. The peaks of scattering angles 2θ values located at *ca.* 26.5°, 43.9°, and 52.1° are attributed to the diffractions of the (111), (220), and (311) facet crystal planes of cubic phase CdS, respectively[30]. No apparent peak for the separate GR in GR-CdS composites is detected in XRD patterns, which is probably because of the relative low intensity of GR at *ca.* 25.0° shielded by the CdS diffraction peak[20,21].

The addition of GR into CdS matrix induces a significant change on the optical property of semiconductor CdS, as displayed in Figure S2 (Supplementary Information). With the increase of GR content, there is an enhanced absorbance in the visible light region ranging from 600 to 800 nm. It is noted that, compared with blank-CdS, the GR-CdS composites show the band gap narrowing trend, *i.e.*, the red shift to higher wavelength, which is evidenced by the plot of transformed Kubelka-Munk function versus the energy of light (Figure S2b). The band gaps of blank-CdS, 1%GR-CdS, 5%GR-CdS, 10%GR-CdS, and 30% GR-CdS are estimated to be *ca.* 2.27 eV, 2.27 eV, 2.26 eV, 2.15 eV and 2.10 eV, respectively, indicating a band gap narrowing of semiconductor CdS after its hybridization with GR.

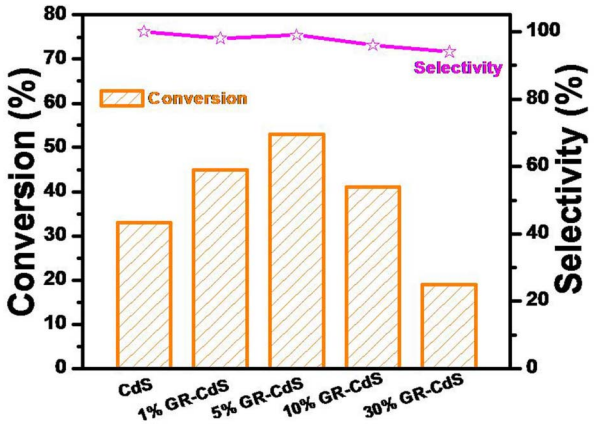

Figure 1 | Photocatalytic selective oxidation of toluene to benzaldehyde over the as-prepared GR-CdS composites and blank-CdS under visible light irradiation of 10 h.

The photoactivity of activation of C–H bond in toluene over GR-CdS composites has been tested using the same reaction condition as that over blank-CdS photocatalyst under visible light irradiation. It can be seen from Figure 1 that, under visible light irradiation of 10 h, 53% conversion of toluene is achieved over the optimal 5%GR-CdS composite, which is much higher than 33% conversion over the blank-CdS photocatalyst under identical reaction conditions. On the other hand, the selectivity to benzaldehyde can still be maintained as high as 99%, indicating that the proper amount addition of GR not only improves the photoactivity of CdS for C–H activation in toluene, but also does not play a significant effect on the achievement of high selectivity to benzaldehyde. The excessive addition of GR, *e.g.*, the 30%GR-CdS sample, will dramatically lower the photoactivity of CdS while the selectivity is decreased moderately. This is mainly because that the higher addition of GR lowers the contact surface of CdS with the light illumination and efficiency of light passing through the depth of the reaction solution, also called a "shielding effect" as widely observed in GR-semiconductor composite photocatalysts[20,21,34]. In the next, when we introduce the second co-catalyst TiO_2 to further improve the photoactivity of CdS catalyst toward C–H activation, the addition ratio of co-catalyst GR is set as 5% to construct ternary GR-CdS-TiO_2 composites (details for synthesis of GR-CdS-TiO_2 in the Supplementary Information).

Figure 2a shows the XRD patterns of ternary 5%GR-CdS-TiO_2 composites with different weight addition ratios of TiO_2. It is seen that, when the weight addition ratio of TiO_2 is low, *i.e.*, 1, 5 and 10% TiO_2, the 5%GR-CdS-TiO_2 composites show similar XRD patterns with that for 5%GR-CdS. When the weight ratio of TiO_2 is increased to 30 and 50%, the characteristic diffraction peaks at 25.3°, 37.8°, and 48.0° are clearly observed, which are attributed to the (101), (004), and (200) facets of anatase TiO_2[35]. According to the calculation based on the Scherrer formula, the average crystallite sizes of CdS and TiO_2 in the GR-CdS-TiO_2 composite are determined to be about 1.9 nm and 5.0 nm, respectively. As expected, with the addition of second co-catalyst TiO_2, the photoactivity toward aerobic oxidation of C–H in toluene is further enhanced as compared to the binary 5%GR-CdS composite, which is evidenced by the photoactive test in Figure 2b. For example, 69% conversion of toluene can be obtained over the optimal ternary 5%GR-CdS-10%TiO_2 composite under visible light irradiation, which is higher than 53% and 33% conversion for that over 5%GR-CdS and blank-CdS photocatalyst, respectively. In addition, to evaluate the stability of photocatalyst, we have performed

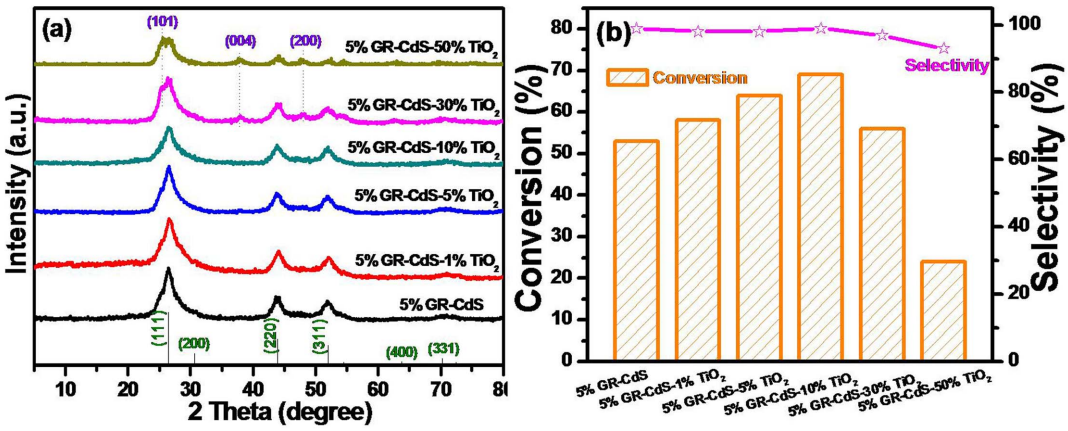

Figure 2 | XRD patterns of GR-CdS-TiO_2 composites and 5%GR-CdS for comparison (a), and their photoactivity toward selective oxidation of toluene to benzaldehyde under visible light irradiation of 10 h (b).

recycling photoactivity test for the 5%GR-CdS and 5%GR-CdS-10%TiO_2 composites. As shown in Figure S3 (Supplementary Information), after 5 times recycling test, no significant loss of photoactivity is observed, because the conversion of toluene over 5%GR-CdS and 5%GR-CdS-10%TiO_2 is similar to the fresh samples while the selectivity to benzaldehyde is maintained > 97%. Therefore, the as-prepared composite samples are stable visible-light-driven photocatalyst for the selective oxidation of toluene in the reaction medium of BTF solvent under ambient conditions. Furthermore, we have also carried out the reaction for oxidation of toluene to benzaldehyde over 5%GR-CdS-10%TiO_2 by extending the reaction time, which is shown in Figure S4 (Supplementary Information). It can be seen that the conversion of toluene is enhanced with the reaction time is progressing. After visible light irradiation of 19 h, the conversion of toluene over 5%GR-CdS-10%TiO_2 is up to 98% while the selectivity to benzaldehye is 95%. In addition, to ensure if this photoactivity enhancement is general, we have performed selective oxidation of other substituted toluenes over these photocatalysts under visible light irradiation. As shown in Table 1, the optimal ternary 5%GR-CdS-10%TiO_2 shows higher photoactivity than both 5%GR-CdS and blank-CdS toward selective oxidation of substituted toluenes to corresponding aldehydes with high selectivity > 98%. Considering the fact that GR, blank-TiO_2 or 5%GR-TiO_2 almost does not have the photoactivity for toluene conversion under identical reaction conditions, as shown in Figure S5 (Supplementary Information), it can be concluded that the primary photoactive ingredient in ternary 5%GR-CdS-10%TiO_2 composite is visible-light-responsive CdS and that the role of GR and TiO_2 acts as co-catalysts to promote the photoactivity enhancement of CdS toward C–H activation in toluene and substituted toluenes. In other words, if these individual components are integrated in a rational manner, these two co-catalysts GR and TiO_2 in the photocatalyst GR-CdS-TiO_2 would cooperate with the light harvester (semiconductor CdS) to facilitate the charge carriers separation/transfer and lengthen the lifetime of photogenerated electron-hole pairs from band-gap-photoexcitation of CdS under visible light irradiation, thereby resulting in an increase in the overall photocatalytic performance. This inference has been faithfully verified by the comparative analysis of photoelectrochemical and photoluminescence (PL) spectra on the optimal 5%GR-CdS-10%TiO_2, 5% GR-CdS and blank-CdS. In the following discussion section, we will show that the enhanced photoactivity is primarily attributed to the improved lifetime and transfer of photogenerated charge carriers. In addition, the possible reaction mechanism for selective oxidation of toluene over the optimal 5%GR-CdS-10%TiO_2 under visible light irradiation is also studied and discussed.

Discussion

As shown in Figure 3a, under visible light irradiation, the photocurrent transient response for 5%GR-CdS is higher than blank-CdS, indicating that the addition of GR as co-catalyst into the semiconductor CdS matrix can improve the lifetime of photogenerated charge carriers. With regard to the optimal

Table 1 | Photocatalytic selective oxidation of substituted toluenes to corresponding aldehydes over blank-CdS, 5%GR-CdS, and 5%GR-CdS-10%TiO_2 under visible light irradiation of 10 h

Catalyst	substrate	product	conv.(%)	sel.(%)
blank-CdS			27	100
5%GR-CdS			52	99
5%GR-CdS-10%TiO_2			66	99
blank-CdS			30	100
5%GR-CdS			54	99
5%GR-CdS-10%TiO_2			68	99
blank-CdS			29	100
5%GR-CdS			51	99
5%GR-CdS-10%TiO_2			65	98
blank-CdS			36	100
5%GR-CdS			57	100
5%GR-CdS-10%TiO_2			71	99
blank-CdS			39	100
5%GR-CdS			58	98
5%GR-CdS-10%TiO_2			73	98

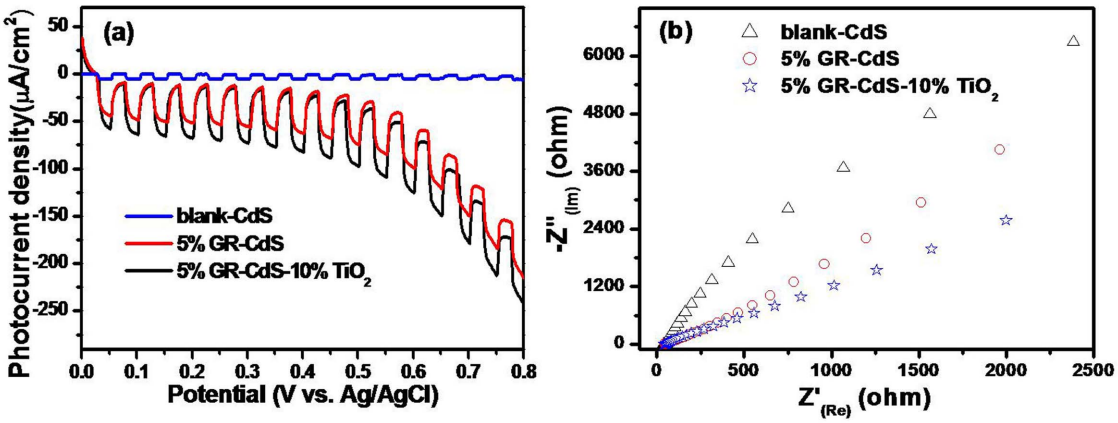

Figure 3 | Chopping photocurrent−voltage curves (a) and Nyquist impedance plots (b) of blank-CdS, 5%GR-CdS and 5%GR-CdS-10%TiO_2 in 0.2 M Na_2SO_4 (pH = 6.8) aqueous solution versus Ag/AgCl under visible light irradiation.

5%GR-CdS-10%TiO_2 under visible light irradiation, the photocurrent transient response is the highest, suggesting that the addition of second co-catalyst TiO_2 is able to further improve the lifetime of photogenerated carriers. Figure 3b shows the electrochemical impedance spectroscopy (EIS) Nyquist plots of the electrode samples of 5%GR-CdS-10%TiO_2, 5%GR-CdS and blank-CdS under visible light irradiation. It is clearly seen that, with the addition of GR and TiO_2, the semi-circle in the plot becomes shorter, which indicates a decrease in the solid state interface layer resistance and the charge transfer resistance on the surface[36]. Thus, the charge carriers transfer over 5%GR-CdS-10%TiO_2 is more efficient than that over 5%GR-CdS and blank-CdS. The PL spectra analysis (Figure S6, Supplementary Information) further shows that, after the coupling of CdS with two co-catalysts GR and TiO_2, the quenching degree of PL intensity is obviously enhanced, suggesting that the lifetime of photogenerated charge carriers over the ternary 5%GR-CdS-10%TiO_2 is the highest among these three samples[37]. Since the conduction band of CdS is more negative than that of TiO_2 or graphene, the transfer of photogenerated electrons from band-gap-photoexcitation of CdS under visible light irradiation to the conduction band of TiO_2 or graphene is energetically favorable, which thus improves the fate and transfer of charge carriers in the ternary 5%GR-CdS-10%TiO_2 system[21,35]. These consequently contribute to the highest photoactivity of 5%GR-CdS-10%TiO_2 toward activation of C–H bonds in toluene and substituted toluenes under visible light irradiation.

To further understand the electron transfer, we have performed the Mott-Schottky plots for GR, blank-TiO_2 and blank-CdS, as displayed in Figure S7 (Supplementary Information). The Fermi level (E_F) of GR and flat band potential (E_{FB}) of TiO_2 and CdS, as calculated from the *X* intercepts of the linear region, are found to be −0.30 V, −0.50 V and −0.71 V *versus* Ag/AgCl (equivalent to −0.10 V, −0.30 V and −0.51 V *versus* normal hydrogen electrode, NHE), respectively. Because of E_F (GR) > E_{CB} (TiO_2) > E_{CB} (CdS), electrons will transfer from the conduction band (CB) of CdS to TiO_2, and then from TiO_2 to GR, thus forming a long-lived electron-transfer state, which is beneficial for the overall photoactivity enhancement and in line with the above PL analysis and photoactivity data.

To learn the microscopic structure and morphology, we have performed the TEM analysis on the optimal ternary 5%GR-CdS-10%TiO_2 composite and the results are displayed in Figure 4. It can be clearly seen that the two co-catalysts GR and TiO_2 are intimately integrated with the semiconductor CdS matrix to form the ternary GR-CdS-TiO_2 composite with a large sheet structure. Such intimate interfacial contact has been well recognized to be a beneficial factor for the charge carriers transfer across the interface[20,21]. The stacking GR layers can be distinctly identified from the high-resolution TEM (HRTEM) image, as displayed in panel b in Figure 4. In addition, two main distinct lattice fringes are clearly distinguished in the HRTEM image. That is, the spacing of 0.336 and 0.352 nm can be ascribed to the (111) and (101) crystal face of cubic phase CdS and anatase TiO_2, respectively. The elemental mapping analysis corresponding to the green line boxed area in panel a of Figure 4 further confirms the coexistence of CdS, TiO_2 and GR, which are evenly distributed in the GR-CdS-TiO_2 composite. In addition, the energy dispersive X-ray (EDX) analysis also confirms the coexistence of CdS, TiO_2 and GR (Figure S8, supplementary information).

To further ensure that the lifetime of photogenerated charge carriers is the most predominant factor determining the overall photocatalytic performance of GR-CdS-TiO_2 toward selective oxidation of C–H bond in toluene, we have performed the specific surface area analysis and the results are listed in Table S1. The surface area of blank-CdS, 5%GR-CdS and 5%GR-CdS-10%TiO_2 is *ca.* 132 $m^2 \cdot g^{-1}$, 128 $m^2 \cdot g^{-1}$ and 139 $m^2 \cdot g^{-1}$, respectively. The adsorption experiment for toluene in the dark also suggests that there is almost no difference in the adsorptivity of these three samples toward toluene (Figure S9, Supplementary Information). These results suggest that the surface area is not the primary factor leading to the large discrepancy in their photoactivities. On the contrary, the lifetime and transfer efficiency of photogenerated electron-hole pairs are the key and predominant factors that determine the overall photocatalytic activity of 5% GR-CdS-10%TiO_2.

To understand the role of photogenerated radical species and underlying reaction mechanism involved for photocatalytic selective oxidation of toluene over the 5%GR-CdS-10%TiO_2 composite under visible light irradiation, we have performed a series of control experiments in the inert N_2 atmosphere and with adding different scavengers for quenching hydroxyl radicals ($^{\bullet}OH$), superoxide radicals ($O_2^{\bullet -}$), holes (h^+), and electrons (e^-), respectively[38,39]. As shown in Figure 5, control experiment in N_2 atmosphere shows only trace conversion of toluene, confirming that oxygen in the reaction system is the primary oxidant for oxidation of toluene. When ammonium oxalate (AO) scavenger for holes is added, the conversion of toluene is almost terminated under visible light irradiation. When benzoquinone (BQ) scavenger for superoxide radicals is added into the reaction system, the conversion of toluene is significantly inhibited. Such a remarkable inhibition on toluene conversion is also observed when $K_2S_2O_8$ scavenger for electrons is added into the reaction system. Although electrons are not able to directly participate in oxidation of toluene, the electrons quenching by the addition of $K_2S_2O_8$ scav-

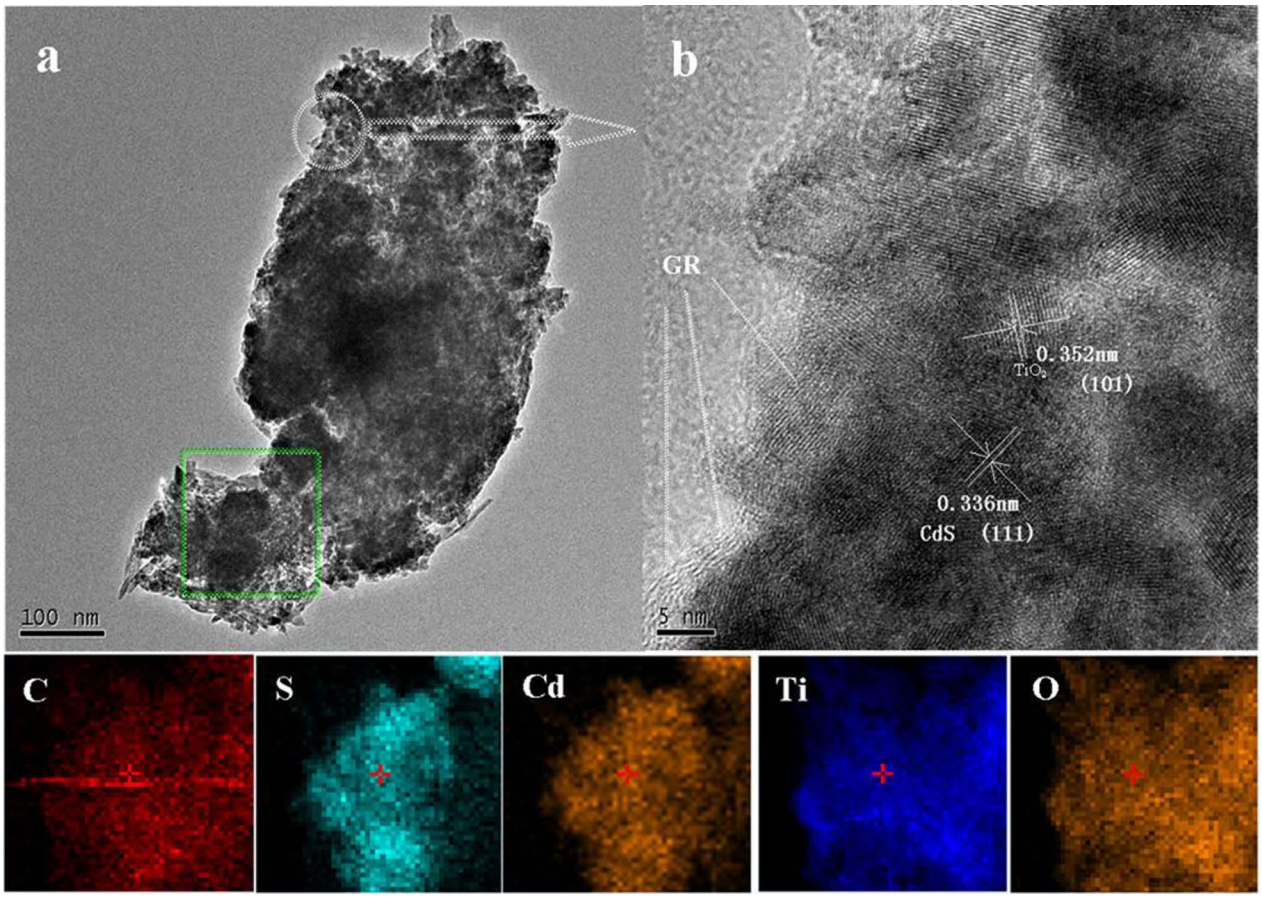

Figure 4 | Typical TEM and high-resolution TEM (HRTEM) images of the optimal 5%GR-CdS-10%TiO_2 composite and elemental mapping patterns (bottom panels) corresponding to the green line boxed area in panel a.

enger will prevent the activation of molecular oxygen; for example, the superoxide radicals are generated from accepting photogenerated electrons by molecular oxygen. Thus, it is understandable to observe the significant inhibition of toluene conversion for both the cases of adding BQ and $K_2S_2O_8$, respectively. The above control experiments clearly suggest that the positively charged holes play the predominant role in photocatalytic oxidation of toluene over 5%GR-CdS-10%TiO_2. The role of negatively charged electrons is to activate molecular oxygen (*e.g.*, the formation of superoxide radicals), which then acts as the primary oxidant for toluene conversion. In addition, it is worth noting that the addition of *tert*-butyl alcohol (TBA) scavenger for hydroxyl radicals plays a negligible effect on toluene conversion, which is in faithful accordance with the absence of hydroxyl radicals in the benzotrifluoride (BTF) solvent and also confirmed by our ESR analysis (Figure S10, Supplementary Information)[20,23].

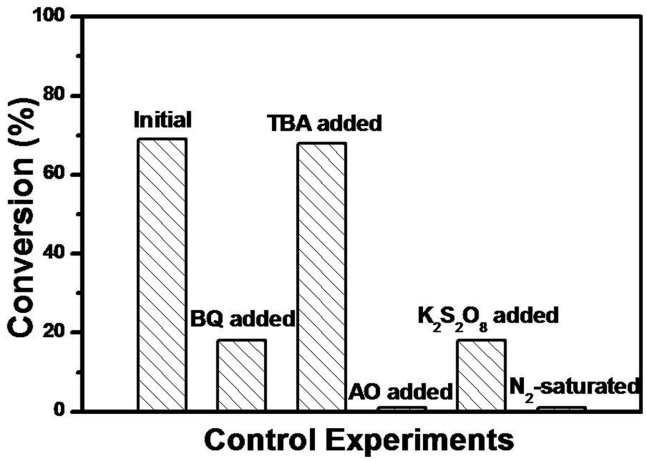

Figure 5 | Control experiments of photocatalytic selective oxidation of toluene in the inert N_2 atmosphere or with the addition of different radical scavengers: benzoquinone (BQ, scavenger for superoxide radicals), *tert*-butyl alcohol (TBA, scavenger for hydroxyl radicals), ammonium oxalate (AO, scavenger for holes) and $K_2S_2O_8$ (scavenger for electrons) over the optimum 5%GR-CdS-10%TiO_2 under visible light irradiation for 10 h.

Based on the above discussions, a tentative photocatalytic reaction mechanism for oxidation of toluene over the 5%GR-CdS-10%TiO_2 composite can be proposed as the following. Under visible light irradiation, the electron-hole pairs are generated from CdS. The adsorbed toluene over the surface of 5%GR-CdS-10%TiO_2 is able to be oxidized to the corresponding cationic radicals by the positive holes with strong oxidation power[30]. The photogenerated electrons from conduction band (CB) of CdS can transfer to TiO_2 and GR, thus forming a long-lived electron-transfer state. Meanwhile, the electrons can react with the adsorbed O_2 to give activated oxygen species (*e.g.*, $O_2^{\bullet-}$). The oxygen or activated oxygen species are then able to selectively oxidize the above cationic radicals, giving rise to the formation of the target product, benzaldehyde.

In summary, we have demonstrated a viable strategy of assembling two co-catalysts, GR and TiO_2, into the semiconductor CdS matrix to form ternary GR-CdS-TiO_2 composites with intimate spatial integration and sheet-like structure. The introduction of dual co-catalysts into the CdS matrix can optimize and improve the separation and transfer of charge carriers over the light harvester CdS under visible light irradiation, by which the visible light photoactivity of CdS for

aerobic C–H activation under mild conditions is obviously enhanced. This work would inspire growing interest in rationally adopting co-catalyst strategy to design more efficient semiconductor-based photocatalyst toward activation of C–H bonds using solar light and benign molecular oxygen. We also expect that further optimization of the chemical compositions and synergetic interaction of GR, CdS and TiO_2 may further improve the photoactivity for C–H activation in the future.

Methods

Materials. All chemicals used in this work were purchased from *Sinopharm Chemical Reagent* Co., Ltd. (Shanghai, China) and *Alfa Aesar*. Details were provided in the supplementary information.

Synthesis. *Synthesis of graphene oxide (GO).* Graphene oxide (GO), the precursor of graphene (GR) in this work, was prepared by a modified Hummers method, which was also used in our previous studies[20,21].

Synthesis of CdS sample. Our CdS sample was prepared by a very simple room temperature method, as reported earlier from our group[30]. Typically, 200 mL of 6.0 mM Na_2S was slowly added into 200 mL of 5.0 mM $Cd(Ac)_2$ in a drop-by-drop process for 4 h, and was aged for 36 h with vigorous stirring. Then, the products were separated by filtration, washed by water, and fully dried at 333 K in oven to get the final CdS sample, which is further used to construct the binary GR-CdS and ternary GR-CdS-TiO_2 nanocomposites.

Synthesis of TiO_2 colloids. 1.32 mL of TBOT was dispersed into 30 mL C_2H_5OH, and airproof was aged for 48 h with vigorous stirring to obtain the TiO_2 colloids, which were used for construct the ternary GR-CdS-TiO_2 nanocomposites.

Synthesis of GR-CdS nanocomposites. Typically, GO was ultrasonicated in 100 mL of deionized water to disperse it well, and then 0.2 g of the as-prepared CdS sample was added to the given amount of the above GO solution to prepare GO-CdS nanocomposites with different weight addition ratios of GO. The mixing solution was aged with vigorous stirring for 24 h to obtain a homogeneous suspension. Then, this suspension was evaporated at water-bath 323 K in vacuum rotary evaporator and fully dried at 333 K in oven. Then, GO-CdS was aged in 40 mL of deionized water with vigorous stirring for 30 min to obtain a homogeneous suspension. After that, it was transferred to 50 mL Teflon-sealed autoclave and maintained at 393 K for 12 h, during which GO was reduced to GR[20,21]. Subsequently, the products were cooled to room temperature and recovered by filtration, washed by water, and fully dried at 333 K in oven to get the final GR-CdS nanocomposites with different weight addition ratios of GR, namely 1, 5, 10, and 30% GR-CdS.

Synthesis of GR-CdS-TiO_2 nanocomposites. Typically, GO was ultrasonicated in 100 mL of deionized water to disperse it well, and then the as-prepared CdS sample and TiO_2 colloids were added to the above GO solution. The mixing solution was aged with vigorous stirring for 24 h to obtain a homogeneous suspension. Then, this suspension was evaporated at water-bath 323 K in vacuum rotary evaporator and fully dried at 333 K in oven. Then, this GO-CdS-TiO_2 sample was aged in 40 mL of deionized water with vigorous stirring for 30 min to obtain a homogeneous suspension. After that, it was transferred to 50 mL Teflon-sealed autoclave and maintained at 393 K for 12 h during which GO was reduced to GR[20,21]. After that, the products were cooled to room temperature and recovered by filtration, washed by water, and fully dried at 333 K in oven to get the final GR-CdS-TiO_2 nanocomposites with different weight addition ratios of TiO_2. Following these steps, a series of GR-CdS-TiO_2 nanocomposites, including 1, 5, 10, 30, and 50% TiO_2-5% GR-CdS were obtained.

Characterization. The optical properties were analyzed by UV-vis diffuse reflectance spectroscopy (DRS) using a UV-vis spectrophotometer (Cary 500, Varian), in which $BaSO_4$ was employed as the internal reflectance standard. The phase composition of the samples was determined by X-ray diffraction (XRD, Philip X′ Pert Pro MPP) using a Cu Kα radiation (λ = 1.5418 Å) at the scan rate of 0.08/s. The photoluminescence (PL) spectra for solid samples were investigated on an Edinburgh FL/FS900 spectrophotometer. The Brunauer-Emmett-Teller (BET) specific surface area was analyzed by nitrogen adsorption in a Micromeritics ASAP 2020 apparatus. The morphology and microscopic structure information was determined by transmission electron microscopy (TEM, FEI Tecnai G2 F20 S-TWIN). For the TEM analysis, the samples were dispersed in ethanol by ultrasonic treatment and dropped on the lacey support film without carbon coating copper grids. The radical species were detected by electron spin resonance (ESR) spectrometer on a Bruker EPR A300 instrument. The parameters for the ESR spectrometer were as follows: center field = 3507 G, microwave frequency = 9.84 GHz, and power = 6.36 mW. The electrochemical analysis was carried out in a conventional three-electrode cell using a Pt plate and an Ag/AgCl electrode as the counter electrode and reference electrode, respectively. The electrolyte was 0.2 M Na_2SO_4 aqueous solution without additive (pH = 6.8). The photocurrent measurements were taken on a BAS Epsilon workstation without bias. The electrochemical impedance spectroscopy (EIS) were conducted on a Precision PARC workstation.

Photocatalytic activity test. Photocatalytic selective oxidation of toluene and substituted toluenes was performed under ambient conditions, *i.e.*, room temperature and atmospheric pressure[23,24,30]. Typically, toluene (0.1 mmol) and 8 mg of the catalyst were dissolved in the solvent of benzotrifluoride (BTF, supplied from Alfa Aesar with a purity of > 99%) (1.5 mL) saturated with pure molecular oxygen from a gas cylinder. Such a standard reaction condition has previously been used for photocatalytic oxidation of alcohols or amines over TiO_2-based semiconductor and graphene-TiO_2 composites[20,23,24,40]. The mixture was transferred into a 10 mL Pyrex glass bottle filled with molecular oxygen at a pressure of 0.1 MPa and stirred for half an hour to make the catalyst blend evenly in the solution. The suspensions were irradiated by a 300 W Xe arc lamp (PLS-SXE 300, Beijing Perfectlight Co. Ltd.) with a UV-CUT filter (λ > 420 nm). After the reaction, the mixture was centrifuged to completely remove the catalyst particles. The remaining solution was analyzed with an Aglient Gas Chromatograph (GC-7820, with a capillary FFAP analysis column). The assignment of products was confirmed by a Hewlett-Packard gas chromatograph/mass spectrometer (HP-5973GC/MS). Controlled photoactivity experiments using different radical scavengers (ammonium oxalate as scavenger for photogenerated holes, $K_2S_2O_8$ as scavenger for electrons, *tert*-butyl alcohol as scavenger for hydroxyl radicals, and benzoquinone as scavenger for superoxide radical species) were performed similar to the above photocatalytic oxidation of toluene except that the radical scavengers (0.1 mmol) were added to the reaction system[30,38,39].

1. Labinger, J. A. & Bercaw, J. E. Understanding and exploiting C–H bond activation. *Nature* **417**, 507–514 (2002).
2. bin Saiman, M. I. *et al.* Involvement of surface-bound radicals in the oxidation of toluene using supported Au-Pd nanoparticles. *Angew. Chem. Int. Ed.* **51**, 5981–5985 (2012).
3. Chen, X., Engle, K. M., Wang, D.-H. & Yu, J.-Q. Palladium(II)-catalyzed C–H activation/C–C cross-coupling reactions: versatility and practicality. *Angew. Chem. Int. Ed.* **48**, 5094–5115 (2009).
4. Chen, M. S. & White, M. C. A predictably selective aliphatic C–H oxidation reaction for complex molecule synthesis. *Science* **318**, 783–787 (2007).
5. Sheldon, R. A. & van Bekkum, H. *Fine chemicals through heterogeneous Catalysis* [Sheldon, R. A. & van Bekkum, H. (ed.)] [1–10] (Wiley-VCH, Weinheim, 2001).
6. Kesavan, V., Sivanand, P. S., Chandrasekaran, S., Koltypin, Y. & Gedanken, A. Catalytic aerobic oxidation of cycloalkanes with nanostructured amorphous metals and alloys. *Angew. Chem. Int. Ed.* **38**, 3521–3523 (1999).
7. Thomas, J. M., Raja, R., Sankar, G. & Bell, R. G. Molecular-sieve catalysts for the selective oxidation of linear alkanes by molecular oxygen. *Nature* **398**, 227–230 (1999).
8. Shilov, A. E. & Shul'pin, G. B. Activation of C–H bonds by metal complexes. *Chem. Rev.* **97**, 2879–2932 (1997).
9. Kesavan, L. *et al.* Solvent-free oxidation of primary carbon-hydrogen bonds in toluene using Au-Pd alloy nanoparticles. *Science* **331**, 195–199 (2011).
10. Li, X. H., Chen, J. S., Wang, X., Sun, J. & Antonietti, M. Metal-free activation of dioxygen by graphene/g-C_3N_4 nanocomposites: functional dyads for selective oxidation of saturated hydrocarbons. *J. Am. Chem. Soc.* **133**, 8074–8077 (2011).
11. Maldotti, A., Molinari, A. & Amadelli, R. Photocatalysis with organized systems for the oxofunctionalization of hydrocarbons by O_2. *Chem. Rev.* **102**, 3811–3836 (2002).
12. Maeda, K., Lu, D. & Domen, K. Oxidation of water under visible-light irradiation over modified $BaTaO_2N$ photocatalysts promoted by tungsten species. *Angew. Chem. Int. Ed.* **52**, 6488–6491 (2013).
13. Maeda, K. & Domen, K. Water oxidation using a particulate $BaZrO_3$-$BaTaO_2N$ solid-solution photocatalyst that operates under a wide range of visible light. *Angew. Chem. Int. Ed.* **51**, 9865–9869 (2012).
14. Tada, H., Kiyonaga, T. & Naya, S. Rational design and applications of highly efficient reaction systems photocatalyzed by noble metal nanoparticle-loaded titanium (IV) dioxide. *Chem. Soc. Rev.* **38**, 1849–1858 (2009).
15. Yurdakal, S., Palmisano, G., Loddo, V., Augugliaro, V. & Palmisano, L. Nanostructured rutile TiO_2 for selective photocatalytic oxidation of aromatic alcohols to aldehydes in water. *J. Am. Chem. Soc.* **130**, 1568–1569 (2008).
16. Palmisano, G. *et al.* Advances in selective conversion by heterogeneous photocatalysis. *Chem. Commun.* **46**, 7074–7089 (2010).
17. Bard, A. J. & Fox, M. A. Artificial photosynthesis: solar splitting of water to hydrogen and oxygen. *Acc. Chem. Res.* **28**, 141–145 (1995).
18. Fox, M. A. Organic heterogeneous phtocatalysis: chemical conversion sensitized by irradiation semiconductors. *Acc. Chem. Res.* **16**, 314–321 (1983).
19. Shiraishi, Y. & Hirai, T. Selective organic transformations on titanium oxide-based photocatalysts. *J. Photochem. Photobiol., C* **9**, 157–170 (2008).
20. Zhang, Y., Tang, Z.-R., Fu, X. & Xu, Y.-J. Engineering the unique 2D mat of graphene to achieve graphene-TiO_2 nanocomposite for photocatalytic selective transformation: what advantage does graphene have over its forebear carbon nanotube? *ACS Nano* **5**, 7426–7435 (2011).
21. Zhang, N., Zhang, Y. & Xu, Y.-J. Recent progress on graphene-based photocatalysts: current status and future perspectives. *Nanoscale* **4**, 5792–5813 (2012).
22. Zhang, N. & Xu, Y.-J. Aggregation- and leaching-resistant, reusable, and multifunctional Pd@CeO_2 as a robust nanocatalyst achieved by a hollow core-shell strategy. *Chem. Mater.* **25**, 1979–1988 (2013).

23. Zhang, M., Chen, C., Ma, W. & Zhao, J. Visible-light-induced aerobic oxidation of alcohols in a coupled photocatalytic system of dye-sensitized TiO_2 and TEMPO. *Angew. Chem., Int. Ed.* **407**, 9730–9733 (2008).
24. Zhang, M. *et al*. Oxygen atom transfer in the photocatalytic oxidation of alcohols by TiO_2: Oxygen Isotope Studies. *Angew. Chem., Int. Ed.* **48**, 6081–6084 (2009).
25. Wang, Q., Zhang, M., Chen, C., Ma, W. & Zhao, J. Photocatalytic aerobic oxidation of alcohols on TiO_2: the acceleration effect of a bronsted acid. *Angew. Chem. Int. Ed.* **49**, 7976–7979 (2010).
26. Lang, X., Ji, H., Chen, C., Ma, W. & Zhao, J. Selective formation of imines by aerobic photocatalytic oxidation of amines on TiO_2. *Angew. Chem., Int. Ed.* **50**, 3934–3937 (2011).
27. Fukuzumi, S. *et al*. Formation of a long-lived electron-transfer state in mesoporous silica-alumina composites enhances photocatalytic oxygenation reactivity. *Proc. Natl. Acad. Sci. USA* **109**, 15572–15577 (2012).
28. Sarina, S. *et al*. Driving selective aerobic oxidation of alkyl aromatics by sunlight on alcohol grafted metal hydroxides. *Chem. Sci.* **3**, 2138–2146 (2012).
29. Yuan, R. *et al*. Chlorine-radical-mediated photocatalytic activation of C–H bonds with visible light. *Angew. Chem. Int. Ed.* **125**, 1069–1073 (2013).
30. Zhang, Y., Zhang, N., Tang, Z.-R. & Xu, Y.-J. Transforming CdS into an efficient visible light photocatalyst for selective oxidation of saturated primary C–H bonds under ambient conditions. *Chem. Sci.* **3**, 2812–2822 (2012).
31. Zhai, Q. *et al*. Photocatalytic conversion of carbon dioxide with water into methane: platinum and copper(I) oxide co-catalysts with a core-shell structure. *Angew. Chem. Int. Ed.* **52**, 5776–5779 (2013).
32. Fan, W., Zhang, Q. & Wang, Y. Semiconductor-based nanocomposites for photocatalytic H_2 production and CO_2 conversion. *Phys. Chem. Chem. Phys.* **15**, 2632–2649 (2013).
33. Maeda, K. *et al*. Photocatalytic overall splitting promoted by two different cocatalysts for hydrogen and oxygen evolution under visible light. *Angew. Chem. Int. Ed.* **49**, 4096–4099 (2010).
34. Xiang, Q., Yu, J. & Jaroniec, M. Graphene-based semiconductor photocatalysts. *Chem. Soc. Rev.* **41**, 782–796 (2012).
35. Liu, S., Zhang, N., Tang, Z.-R. & Xu, Y.-J. Synthesis of one-dimensional CdS@ TiO_2 core-shell nanocomposites photocatalyst for selective redox. The dual role of TiO_2 shell. *ACS Appl. Mater. Interfaces* **4**, 6378–6385 (2012).
36. Wang, D. *et al*. Self-assembled TiO_2-graphene hybrid nanostructures for enhanced Li-ion insertion. *ACS Nano* **3**, 907–914 (2009).
37. Xu, Y.-J., Zhuang, Y. & Fu, X. New insight for enhanced photocatalytic activity of TiO_2 by doping carbon nanotubes: A case study on degradation of benzene and methyl orange. *J. Phys. Chem. C* **114**, 2669–2676 (2010).
38. Zhang, Y., Chen, Z., Liu, S. & Xu, Y.-J. Size effect induced activity enhancement and anti-photocorrosion of reduced graphene oxide/ZnO composites for degradation of organic dyes and reduction of Cr(VI) in water. *Appl. Catal. B* **140–141**, 598–607 (2013).
39. Zhang, Y., Zhang, N., Tang, Z.-R. & Xu, Y.-J. Identification of Bi_2WO_6 as a highly selective visible-light photocatalyst toward oxidation of glycerol to dihydroxyacetone in Water. *Chem. Sci.* **4**, 1820–1824 (2013).
40. Lang, X., Ji, H., Chen, C., Ma, W. & Zhao, J. Selective formation of imines by aerobic photocatalytic oxidation of amines on TiO_2. *Angew. Chem., Int. Ed.* **50**, 3934–3937 (2011).

Acknowledgments

The support by the NSFC (20903022, 20903023, 21173045), the Award Program for Minjiang Scholar Professorship, and the NSF of Fujian Province for Distinguished Young Investigator Grant (2012J06003) is gratefully acknowledged.

Author contributions

M.-Q.Y., Y.Z. and N.Z. conducted the experiments. Z.-R.T. analyzed the data and discussed the results. Y.-J.X. wrote the whole manuscript.

Additional information

Supplementary information accompanies this paper at http://www.nature.com/scientificreports

Competing financial interests: The authors declare no competing financial interests.

How to cite this article: Yang, M.-Q., Zhang, Y.H., Zhang, N., Tang, Z.-R. & Xu, Y.-J. Visible-Light-Driven Oxidation of Primary C–H Bonds over CdS with Dual Co-catalysts Graphene and TiO_2. *Sci. Rep.* **3**, 3314; DOI:10.1038/srep03314 (2013).